Solid–Liquid Phase Transitions of Triglycerides in Griebenschmalz, Smalec, and Fedt Studied Using ¹³C Solid-State NMR with

Citation for the original published paper (version of record):
Bernin, D., Leventaki, E., Topgaard, D. (2023). Solid–Liquid Phase Transitions of Triglycerides in Griebenschmalz, Smalec, and Fedt Studied
Using ¹³C Solid-State NMR with Dynamics-Based Spectral Filtering. Applied Magnetic Resonance, 54(11-12): 1165-1175. http://dx.doi.org/10.1007/s00723-023-01564-5

Applied Magnetic Resonance
https://doi.org/10.1007/s00723-023-01564-5

Applied Magnetic Resonance

ORIGINAL PAPER

Solid–Liquid Phase Transitions of Triglycerides in *Griebenschmalz*, *Smalec*, and *Fedt* Studied Using ^{13}C Solid-State NMR with Dynamics-Based Spectral Filtering

Diana Bernin[1] · Emmanouela Leventaki[1] · Daniel Topgaard[2]

Received: 15 June 2023 / Revised: 19 June 2023 / Accepted: 7 July 2023

Abstract

The consumer satisfaction of lard-based bread spreads depends on a delicate balance between a liquid fat phase, allowing the spread to flow, and solid fat crystals, providing the product with substance sometimes further enhanced by crispy pork cracklings. Here we apply ^{13}C solid-state NMR with dynamics-based spectral filtering to characterize and follow the temperature dependence of the co-existing solid and liquid triglyceride phases in commercial German *Griebenschmalz* and Polish *smalec*, both containing cracklings, as well as home-made Danish *fedt* and, as a chemically more pure reference, German *Schweineschmalz* intended for baking. The NMR method allows detection of carbon atoms representative of saturated, unsaturated, and polyunsaturated acyl chains in both solid and liquid states. The results show that the solid comprises multiple crystal forms with different melting temperatures, while the liquid is at low temperature enriched in triglycerides with shorter acyl chains and higher degree of unsaturation, which become diluted with long-chain saturated triglycerides as the solids are melting. The obtained deeper understanding of the concomitant aspects of the phase transitions may pave the way for future efforts of rational optimization of fat blend composition to extend the temperature range over which the product contains sufficient amounts of both solids and liquids to give texture properties appealing to consumers.

Prepared for Applied Magnetic Resonance issue on the occasion of Bernhard Blümich’s 70th birthday.

✉ Daniel Topgaard
daniel.topgaard@fkem1.lu.se

[1] Department of Chemistry and Chemical Engineering, Chalmers University of Technology, Göteborg, Sweden

[2] Department of Chemistry, Lund University, Lund, Sweden

1 Introduction

Lard with crispy pieces of skin was the premier bread spread before being all but replaced by butter and margarine in the mid-1900s. The product is known as *Griebenschmalz* in German, *smalec* in Polish, and *fedt* in Danish. Global ambitions of energy conservation and resource utilization have led to a revival of lard as a raw material for food products [1]. Consumer satisfaction depends not only on the taste, but also critically relies on the mouthfeel, which is largely determined by the gradual transitions between various solid and liquid fat phases during biting, chewing, and swallowing. While an individual batch of lard may comprise triglycerides with acyl chain lengths or degrees of unsaturation yielding suboptimal melting behavior, a product with improved customer appeal could be achieved by blending multiple batches as well as including minor amounts of additives that stabilize the melt or certain crystal forms.

For a pure saturated triglyceride system, crystallization from the melt takes place by formation of the metastable pseudohexagonal α-form and subsequently transition to the stable triclinic β-form, sometimes via the orthorhombic β′-form [2, 3]. Simple mixed triglycerides often feature the same general sequence of events with the additional mechanism of fractionation of molecules with different chain lengths in the liquid→α and α→β transitions as illustrated in Fig. 1 [4]. More complex mixtures, including triglycerides with different acyl chain lengths and degrees of unsaturation connected to the same glycerol moiety, can be expected to include even

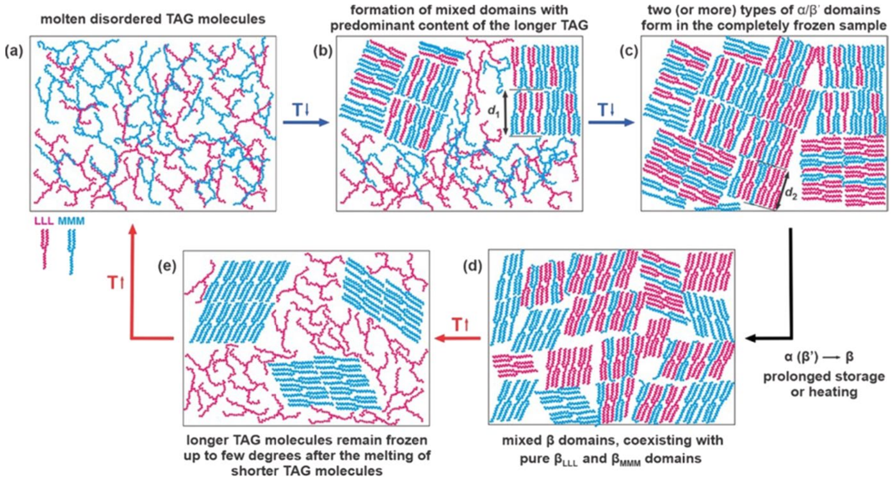

Fig. 1 Schematics of fat crystal forms and phase transitions induced by temperature changes in a two-component system comprising the triglycerides (triacyl glycerols, TAGs) trilaurin (LLL) and trimyristin (MMM) with short and long hydrocarbon chains, respectively. **a** High-temperature liquid mixture. **b** Temperature decrease: liquid–solid co-existence with partial fractionation of the long-chain triglycerides into α-form crystals. **c** Additional temperature decrease: fully crystallized system with multiple crystal forms having varying proportions of short- and long-chain triglycerides. **d** Storage or annealing: partial recrystallization to thermodynamically stable β-form crystals with single types of triglycerides. **e** Heating: co-existence of short-chain liquid and long-chain β-form crystals. Reproduced from Ref [4] with permission from the American Chemical Society

more complex crystallization behavior with fractionation of molecular components between the melt and multiple (meta)stable crystal forms.

While X-ray diffraction gives a wealth of information about crystal symmetries, repeat distances, and, sometimes, atom positions within the unit cell in triglyceride system [3, 5–7], it faces great challenges in characterizing the liquid and the less-ordered solid phases in the multicomponent fat mixtures of relevance for the food industry. Likewise, low-field ^{1}H NMR is a rapid and accurate method for quantifying the ratio between solid and liquid fat [8] but is confounded by the presence of other organic solids, such as pork cracklings, in addition to the fat crystals.

With the aim of enabling rational blending of lard-based spreads, we here apply ^{13}C solid-state NMR with dynamics-based spectral editing [9–11] for detailed characterization of thermotropic phase transitions in store-bought and home-made lard products. The method, illustrated in Fig. 2, relies on magic-angle spinning (MAS) [12] and high-power ^{1}H decoupling to give ^{13}C spectra with sufficient resolution to identify multiple aliphatic, olefinic, and allylic carbons in the hydrocarbon chains [13, 14] even in the presence of skin proteins [15]. Spectral editing by cross-polarization (CP) [16] and insensitive nuclei enhanced by polarization transfer (INEPT) [17], with interpretation of signal intensities within a two-step model of C–H bond reorientation [18, 19] under moderate MAS, allows identification of molecular segments having combinations of

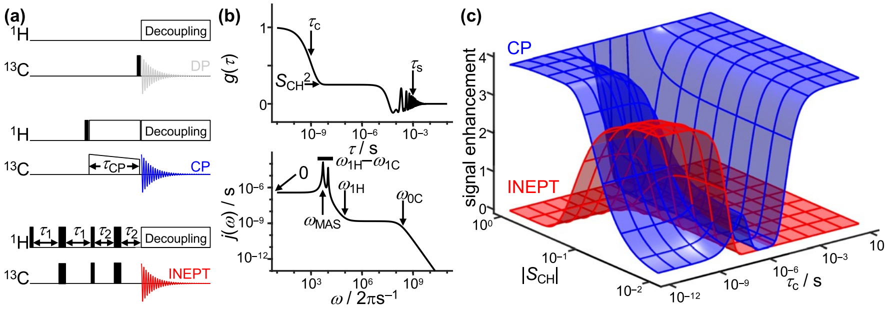

Fig. 2 Principles of ^{13}C MAS NMR spectroscopy with dynamics-based spectral filtering. **a** Diagrams of the pulse sequences DP, ramped CP, and refocused INEPT, wherein the ^{13}C signal is detected during gated ^{1}H decoupling and continuous sample spinning at the frequency ω_{MAS}. Narrow and broad vertical lines symbolize 90° and 180° RF pulses applied at the ^{1}H and ^{13}C Larmor frequencies $\omega_{0\mathrm{H}}$ and $\omega_{0\mathrm{C}}$. CP is performed by simultaneous application of ^{1}H and ^{13}C RF pulses of duration τ_{CP} and with amplitudes giving nutation frequencies $\omega_{1\mathrm{H}}$ and $\omega_{1\mathrm{C}}$ covering the matching conditions $|\omega_{1\mathrm{H}} - \omega_{1\mathrm{C}}|/\omega_{\mathrm{MAS}} = 1$ and/or 2. In the INEPT sequence, conversions from in-phase to anti-phase ^{1}H and anti-phase to in-phase ^{13}C coherences occur during the delays τ_1 and τ_2. Longitudinal relaxation takes place during the recycle delay τ_{R} (not shown) between the end of signal detection and the following 90° pulse. **b** Correlation function $g(\tau)$ and spectral density $j(\omega)$ for the two-step C-H bond reorientation model with MAS wherein $g(\tau)$ decays in two exponential steps with the time constant τ_{c} and τ_{s} separated by an intermediate plateau given by the C–H bond order parameter S_{CH}. Sample spinning yields modulations of $g(\tau)$ at the frequencies ω_{MAS} and $2\omega_{\mathrm{MAS}}$. **c** Theoretical CP (blue) and INEPT (red) signal enhancement as a function of τ_{c} and $|S_{\mathrm{CH}}|$ at constant $\tau_{\mathrm{s}} = 1$ ms calculated for a CH$_2$ segment using the experimental parameters $\omega_{0\mathrm{C}}/2\pi = 125$ MHz, $\omega_{\mathrm{MAS}}/2\pi = 5$ kHz, $\tau_{\mathrm{CP}} = 1$ ms, $\omega_{1\mathrm{H}}/2\pi = 100$ kHz, $(\omega_{1\mathrm{H}}-\omega_{1\mathrm{C}})/\omega_{\mathrm{MAS}}$ ramped from 2.5 to 0.5, $\tau_1 = 1.8$ ms, and $\tau_2 = 1.2$ ms. Adapted from Ref [11] with permission from the authors

correlation times τ_c and order parameters S_{CH} that are classified as solid, intermediate, liquid, and liquid crystalline dynamics [20, 21].

2 Materials and Methods

Schweineschmalz and griebenschmalz were bought in a local Swabian butcher shop in southwestern Germany. The smalec produced by the company Skwierzyna was bought from a Polish food store in Gothenburg, Sweden. The Danish fedt was homemade from two different types of salami (pepper and pepperoni) manufactured by the Danish producer GØL and bought in a supermarket in Lund, Sweden. Salami pieces were fried in a pan until being very crispy and the fat was collected and allowed to solidify at room temperature. All products were used without further purification and stored for weeks at + 4 °C before being prepared for NMR. The samples were placed in disposable HRMAS rotor inserts and transferred to 4 mm zirconia rotors (both from Bruker). The inserts are made from polychlorotrifluoroethylene thermoplastic (trade name: Kel-F) and have a sealed sample volume of approximately 40 µL.

NMR experiments were performed on a Bruker Avance Neo spectrometer operating at the Larmor frequencies $\omega_{0C}/2\pi = 125$ MHz and $\omega_{0H}/2\pi = 500$ MHz for ^{13}C and ^{1}H, respectively. The ^{13}C signal was recorded on a 4 mm HX CPMAS probe at 5 kHz MAS using 400 ppm spectral width, 62 kHz SPINAL-64 ^{1}H decoupling [22], 50 ms acquisition time, accumulation of 256 transients, and $\tau_R = 5$ s with the DP, ramped CP [16, 23], and refocused INEPT [17, 24] sequences displayed in Fig. 2. Hard radiofrequency (RF) pulses were applied at 80 kHz nutation frequencies for both ^{13}C and ^{1}H. CP was performed with the nutation frequencies $\omega_{1C}/2\pi = 60$ kHz and $\omega_{1H}/2\pi$ ramped from 80 to 40 kHz during the contact time $\tau_{CP} = 1$ ms. The delays $\tau_1 = 1.8$ ms, and $\tau_2 = 1.2$ ms were employed for INEPT.

The sample temperature was calibrated by ^{1}H spectra for an external reference of methanol [25] at 5 kHz MAS. After an initial equilibration of the fat samples at − 8 °C for 1 h, data was acquired as a function of temperature in increments of 5 °C with 5 min equilibration after each temperature change before starting the sequence of DP, CP, and INEPT measurements lasting ~ 1 h.

Data was processed in Topspin 4.0 using zero-filling from 5000 to 16,384 points, exponential apodization yielding 20 Hz line broadening, Fourier transformation, and manual phase correction. The ^{13}C chemical shift scale was internally referenced to 14.0 ppm for the terminal CH_3 in the 32 °C INEPT spectrum [26]. INEPT peak areas were estimated by deconvolution using the 'Lorentzian–Gaussian' shape option in MestReNova (Version 14.2.0) after baseline correction using the 'Whittaker Smoother' option.

3 Results and Discussion

Figure 3 shows ^{13}C NMR spectra of griebenschmalz at 2 °C where the comparable amplitudes of the CP and INEPT resonance lines indicate that the sample contains similar amounts of solids and liquids. According to the theoretical signal intensities in Fig. 2c, INEPT is observed for C–H bonds with reorientational correlation time τ_c smaller than ~ 10 ns and order parameter $|S_{CH}|$ lower than ~ 0.2, while CP is efficient in roughly the complementary area of the 2D τ_c-$|S_{CH}|$ space. Exceptions to this simple rule for distinguishing between solids and liquids are the intermediate ($\tau_c \approx 1$ µs and $|S_{CH}| < 0.95$) and liquid crystalline ($\tau_c < 10$ ns and $|S_{CH}| \approx 0.1$) regimes where either none or both of CP and INEPT are efficient [21].

Based on literature data [14, 27], the resonance lines in Fig. 3 were associated to carbon atoms representative of the ends (ω, $\omega - 1$, and $\omega - 2$) and beginnings (1, 2, and 3) of the acyl chains, the glycerol moiety (g1, g2, g3), and acyl chains with double bonds (o1, o2, l1, l2, l3, and l4), including the special case of the two non-conjugated double bonds (l3 and l4) typical for linoleic acid [14]. Since all spectra are acquired with the same spectral width, acquisition time, MAS frequency, and high-power ^{1}H decoupling, as well as processed with the same moderate apodization, the larger linewidths in CP mainly reflect the spread of isotropic chemical shifts originating from a distribution of non-interchanging conformations and packings of otherwise chemically identical molecular segments in the poorly crystalline solids [28, 29]. Conversely, conformational isomerization at rates far exceeding the intrinsic chemical shift-induced frequency differences, for instance ~ 5 ppm × 125 MHz = 625 Hz for the trans and gauche conformations of the saturated hydrocarbon chains [30, 31], results in narrow INEPT peaks with resolution limited by the 50 ms acquisition time and the 20 Hz line broadening required to avoid truncation artifacts. The chemical shift difference between the interior methylene peaks for the solid (all-trans) and liquid (trans/gauche) fat mainly reflects the fractional populations of the various conformational isomers in the two aggregation states [31].

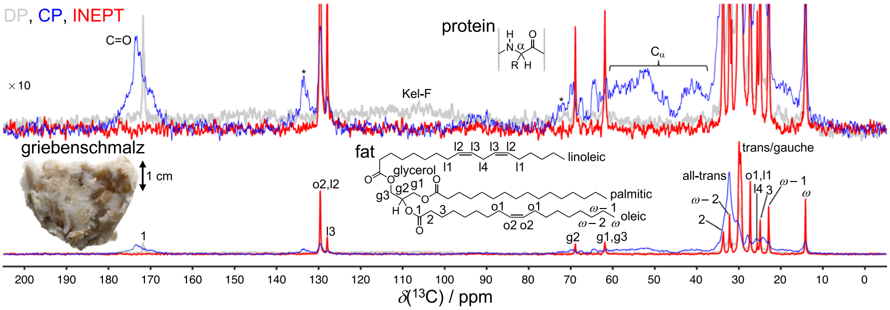

Fig. 3 ^{13}C MAS NMR data of griebenschmalz at + 2 °C using dynamics-based spectral editing to highlight the co-existence of solids and liquids. The data was acquired at $\omega_{0C}/2\pi = 125$ MHz, $\omega_{MAS}/2\pi = 5$ kHz, 62 kHz SPINAL-64 ^{1}H decoupling, and $\tau_R = 5$ s with the DP (gray), CP (blue), and INEPT (red) sequences in Fig. 2a using a ~ 40 µL sample of a fat-embedded pork crackling taken from the commercial product in the photo to the bottom left. CP was performed with $\tau_{CP} = 1$ ms, $\omega_{1C}/2\pi = 60$ kHz, and $\omega_{1H}/2\pi$ ramped from 80 to 40 kHz, while $\tau_1 = 1.8$ ms, and $\tau_2 = 1.2$ ms were used for INEPT. Peak assignments refer to the labeled carbon atoms in the chemical structure drawings of the generic amino acid residue in the protein and a representative fat molecule with linoleic, palmitic, and oleic acyl chains attached via ester bonds to the glycerol moiety. The labels at ~ 30 and ~ 32 ppm point out the distinct chemical shifts of interior methylene segments undergoing trans/gauche conformational isomerization or adopting a straight all-trans configuration as illustrated in Fig. 1e. The top spectra are magnified × 10 compared to the bottom ones. Stars indicate spinning sidebands and the label at 105 ppm shows the maximum of a broad DP resonance from the Kel-F material of the rotor insert

Differences in melting behavior of the fat blends are apparent in the variable temperature data in Fig. 4. The overall balance between solid and liquid fat is estimated by comparison of the all-trans CP and trans/gauche INEPT peaks at ~ 32 and ~ 30 ppm, respectively. At the lowest investigated temperature –8 ºC, all samples are dominated by solid fat, but also contain a substantial liquid fraction increasing in the order schweineschmalz < griebenschmalz ≈ smalec < fedt. With increasing temperature, solid fat is gradually replaced with liquid while preserving the relative order between the samples. All samples contain both solid and liquid fat over a temperature interval spanning more than 40 ºC consistent with a mixture of multiple components with individual transition temperatures determined by their acyl chain lengths and degrees of unsaturation. Closer inspection of the CP and INEPT resonance lines shows differences in chemical shift and linewidth for all types of carbons, including o2/l2, l3, and *ω*, implying that all types of acyl chains occur in both solid and liquid states. Conversely, none of the samples feature the characteristic peaks of anisotropic liquid crystals—CP and INEPT with similar amplitudes at identical chemical shifts and lineshapes [20]—as often observed for phospholipid bilayers with molten acyl chains [32–38]. The absence of these distinctive pairs of CP and INEPT peaks at all investigated temperatures contradicts the sometimes suggested lamellar order in liquid fat just above the melting point [2, 3].

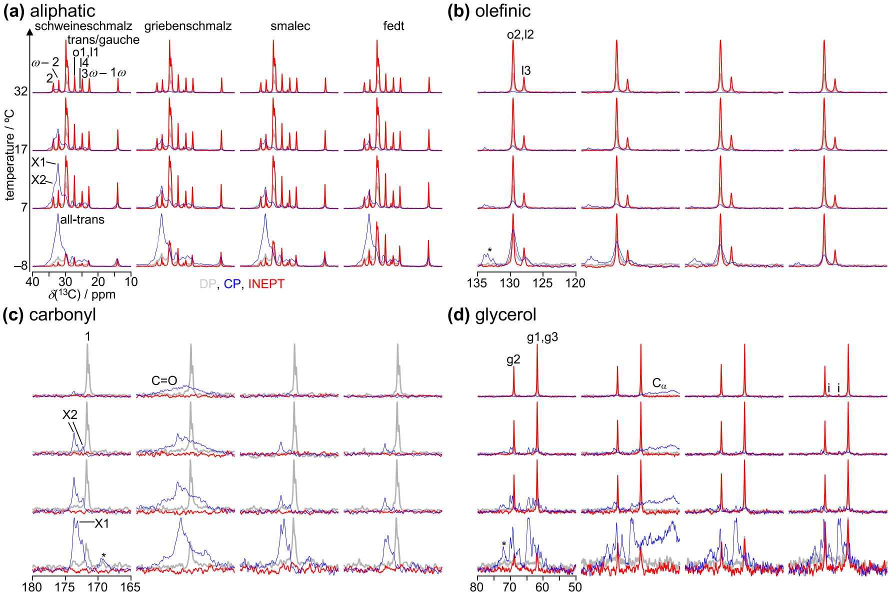

Fig. 4 Variable temperature ^{13}C MAS NMR data for lard-based spreads with zoom-in on chemical shift ranges dominated by **a** aliphatic, **b** olefinic, **c** carbonyl, and **d** glycerol carbons. For each shift range, the spectra are organized in columns for the samples schweineschmalz, griebenschmalz, smalec, and fedt, as well as rows for the selected temperatures –8, 7, 17, and 32 ºC. The DP, CP, and INEPT spectra are jointly scaled to the same maximum intensity for each combination of sample, temperature, and shift range. Peak assignments refer to the carbon labels in Fig. 3 except for X1 and X2, indicating aliphatic and carbonyl peaks originating from different crystal forms, and i from non-triglyceride impurities

More detailed inspection of the temperature dependence of the CP resonances from all-trans methylene at ~ 32 ppm and carbonyl at ~ 173 ppm in Fig. 4 reveals at least two sets of peaks tentatively originating from crystal forms analogous to the low-melting α- and high-melting β-forms found in pure triglyceride systems [7]. While the ~ 1 ppm higher shift of the all-trans methylene for the high-melting form agrees with literature data for the α/β′- and β-forms of tripalmitin [13], and corresponds to the differences observed for the interior methylene carbons in triclinic and other crystal forms of all-trans alkanes [39], the carbonyl shifts are not consistent with the conventional α- (171.9 ppm), β′- (172.5 and 173.3 ppm), or β-forms (172.9, 173.4, and 174.6 ppm) [13, 40], indicating that the molecular conformations and crystal structures in the present fat blends differ from those found in pure triglycerides. Although X-ray diffraction of complex fat blends is often interpreted using crystal form terminology developed for simpler triglyceride systems [41, 42], the data in Fig. 4 suggest that further solid-state NMR studies may be useful to elucidate the details of the structures and possibly identify sub-groups of crystal forms. Contrary to the temperature-sensitivity of the fat, the CP resonances from the protein remain nearly unaffected by the temperature changes as previously observed for skin proteins at dry conditions [15]. Although the general trends of the melting of the solid phases can be estimated from the CP spectra in Fig. 4, actual quantification of the relative proportions of the phases would require recycle delays on the order of a minute to compensate for the unusually slow ^{1}H longitudinal relaxation for the β-form of long-chain saturated triglycerides [40], as well as specialized pulse sequences being less sensitive to differences in relaxation and buildup rates during the CP block [43].

In Fig. 5, the temperature dependence of the composition of the liquid phase can be gleaned from the INEPT peak areas normalized by the value for the terminal methyl groups (ω), which can be expected to melt at lower temperature than any of the other parts of the fat molecules—possibly even being present as liquid-like end-group regions in otherwise solid fat crystals [3]. While the normalized area for the penultimate methylene ($\omega - 1$) remains nearly constant at unity, the values for the interior methylene carbons increase and the olefinic (o2, l2, l3) and allylic (o1, l1, l4) carbons decrease with temperature, showing that the low-temperature fluid is enriched in fat components with short acyl chains and high degree of unsaturation. At the highest temperatures, where all fat is liquid, the peak areas report on the

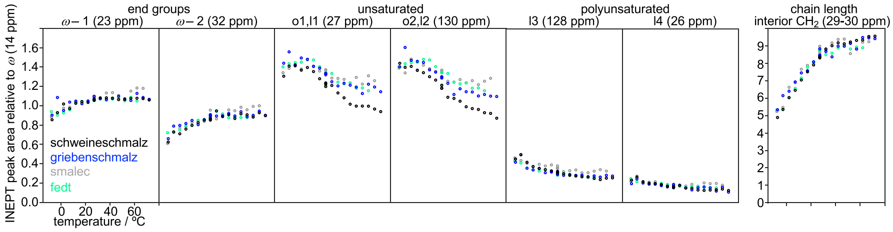

Fig. 5 Temperature dependence of the area of selected INEPT peaks relative to the value for the terminal methyl group ω. The carbon atom labels are explained in Fig. 3 and approximate chemical shifts are given in parenthesis. All panels are shown with the same temperature axis

overall chemical composition. The lowest degree of unsaturation is observed for schweineschmalz, which also has the lowest fraction of liquid at low temperature. Conversely, the higher fraction of liquid for fedt may not be attributed to any differences in acyl chain length or unsaturation, but rather to the thermodynamic mechanism of freezing-point depression induced by the presence of low molecular weight impurities labeled in Fig. 4d. More accurate quantification of the liquid composition could be achieved by systematic variation of the τ_1 and τ_2 delays in the INEPT sequence to account for the dynamics, scalar couplings, and multiplicities of the different carbons at the expense of an order of magnitude longer measurement times [44].

4 Conclusions

Solid-state NMR with dynamics-based spectral filtering enables detailed characterization of co-existing solid and liquid phases in lard-based spreads over wide temperature ranges, showing enrichment of fat components with shorter acyl chains and higher degrees of unsaturation in the low-temperature liquid, the higher melting points of crystal forms with more efficient acyl chain packing, the freezing-point depression induced by low molecular weight impurities, and the minimal effects of temperature on pork cracklings embedded in the fat. These rich details may prove useful for the development of lard products with optimal balance between solid and liquid fractions to achieve favorable texture properties and consumer appeal over an extended range of serving temperatures.

Author Contributions DB and EL prepared samples. EL and DT performed NMR experiments. DB and DT analyzed data, prepared figures, and wrote the main manuscript text. All authors reviewed the manuscript.

Funding Open access funding provided by Lund University. NMR equipment was funded by grants from the Swedish Research Council and the Knut and Alice Wallenberg Foundation.

Availability of Data and Materials Data is available from the authors upon reasonable request.

Declarations

Conflict of Interest The authors declare that they have no conflict of interest.

Ethical Approval Not applicable.

References

1. M. Alm, Animal fats, https://lipidlibrary.aocs.org/edible-oil-processing/animal-fats. (**Accessed: 2023-06-14**)
2. K. Larsson, Molecular arrangement in glycerides. Fette Seifen Anstrichm. **74**, 136–142 (1972). https://doi.org/10.1002/lipi.19720740302
3. L. Hernqvist, K. Larsson, On the crystal structure of the β′-form of trigycerids and structural changes at the phase transitions LIQ. → α → β′ → β. Fette Seifen Anstrichm. **9**, 349–354 (2002). https://doi.org/10.1002/lipi.19820840905
4. D. Cholakova, S. Tcholakova, N. Denkov, Polymorphic phase transitions in bulk triglyceride mixtures. Cryst. Growth Des. **23**, 2075–2091 (2023). https://doi.org/10.1021/acs.cgd.2c01021
5. L.H. Jensen, A.J. Mabis, Crystal structure of β-tricarpin. Nature **197**, 681–682 (1963). https://doi.org/10.1038/197681d0
6. K. Larsson, On the crystal structure of 2-monolaurin. Ark. Kemi **23**, 23–27 (1964)
7. K. Larsson, Classification of glyceride crystal forms. Acta Chem. Scand. **20**, 2255–2260 (1966). https://doi.org/10.3891/acta.chem.scand.20-2255
8. J. Clifford, Investigation of melting and freezing of glycerides by nuclear magnetic resonance spectroscopy. Nature **195**, 568–570 (1962). https://doi.org/10.1038/195568a0
9. I. Matlahov, P.C.A. van der Wel, Hidden motions and motion-induced invisibility: dynamics-based spectral editing in solid-state NMR. Methods **148**, 123–135 (2018). https://doi.org/10.1016/j.ymeth.2018.04.015
10. A. Pandit, Structural dynamics of light harvesting proteins, photosynthetic membranes, and cells observed by spectral editing solid-state NMR. J. Chem. Phys. **157**, 025101 (2022). https://doi.org/10.1063/5.0094446
11. D. Topgaard, Skin, soap, and spaghetti: investigations of co-existing solid and liquid phases in organic materials using solid-state NMR with dynamics-based spectral editing. Pure Appl. Chem. https://doi.org/10.1515/pac-2023-0108. (**in press**)
12. E.R. Andrew, A. Bradbury, R.G. Eades, Removal of dipolar broadening of nuclear magnetic resonance spectra of solids by specimen rotation. Nature **183**, 1802–1803 (1959). https://doi.org/10.1038/1831802a0
13. S.M. Bociek, S. Ablett, I.T. Norton, A ^{13}C-NMR study of the crystal polymorphism and internal mobilities of the triglycerides, tripalmitin and tristearin. J. Am. Oil Chem. Soc. **62**, 1261–1266 (1985). https://doi.org/10.1007/BF02541839
14. Z.O. Oyman, W. Ming, R. van der Linde, Oxidation of ^{13}C-labeled ethyl linoleate monitored and quantitatively analyzed by ^{13}C NMR. Eur. Polym. J. **42**, 1342–1348 (2006). https://doi.org/10.1016/j.eurpolymj.2005.12.003
15. S. Björklund, A. Nowacka, J.A. Bouwstra, E. Sparr, D. Topgaard, Characterization of stratum corneum molecular dynamics by natural-abundance ^{13}C solid-state NMR. PLOS One. **8**, e61889 (2013). https://doi.org/10.1371/journal.pone.0061889
16. A. Pines, J.S. Waugh, M.G. Gibby, Proton enhanced nuclear induction spectroscopy—method for high-resolution NMR of dilute spins in solids. J. Chem. Phys. **56**, 1776–1777 (1972). https://doi.org/10.1063/1.1677439
17. G.A. Morris, R. Freeman, Enhancement of nuclear magnetic resonance signals by polarization transfer. J. Am. Chem. Soc. **101**, 760–762 (1979). https://doi.org/10.1021/ja00497a058
18. H. Wennerström, B. Lindman, O. Söderman, T. Drakenberg, J.B. Rosenholm, ^{13}C magnetic relaxation in micellar solutions. Influence of aggreagte motion on T_1, J. Am. Chem. Soc. **101**, 6860–6864 (1979). https://doi.org/10.1021/ja00517a012
19. G. Lipari, A. Szabo, Model-free approach to the interpretation of nuclear magnetic resonance relaxation in macromolecules. 1. Theory and range of validity. J. Am. Chem. Soc. **104**, 4546–4559 (1982). https://doi.org/10.1021/ja00381a009
20. A. Nowacka, P.C. Mohr, J. Norrman, R.W. Martin, D. Topgaard, Polarization transfer solid-state NMR for studying surfactant phase behavior. Langmuir **26**, 16848–16856 (2010). https://doi.org/10.1021/la102935t
21. A. Nowacka, N.A. Bongartz, O.H.S. Ollila, T. Nylander, D. Topgaard, Signal intensities in ^{1}H–^{13}C CP and INEPT MAS NMR of liquid crystals. J. Magn. Reson. **230**, 165–175 (2013). https://doi.org/10.1016/j.jmr.2013.02.016

22. B.M. Fung, A.K. Khitrin, K. Ermolaev, An improved broadband decoupling sequence for liquid crystals and solids. J. Magn. Reson. **142**, 97–101 (2000). https://doi.org/10.1006/jmre.1999.1896
23. G. Metz, X. Wu, S.O. Smith, Ramped-amplitude cross polarization in magic-angle-spinning NMR. J. Magn. Reson. A **110**, 219–227 (1994). https://doi.org/10.1006/jmra.1994.1208
24. D.P. Burum, R.R. Ernst, Net polarization transfer via a *J*-ordered state for signal enhancement of low-sensitivity nuclei. J. Magn. Reson. **39**, 163–168 (1980). https://doi.org/10.1016/0022-2364(80)90168-7
25. A.L. Van Geet, Calibration of methanol nuclear magnetic resonance thermometer at low temperature. Anal. Chem. **42**, 679–680 (1970). https://doi.org/10.1021/ac50158a064
26. S.V. Dvinskikh, V. Castro, D. Sandström, Heating caused by radiofrequency irradiation and sample rotation in ^{13}C magic angle spinning NMR studies of lipid membranes. Magn. Reson. Chem. **42**, 875–881 (2004). https://doi.org/10.1002/mrc.1477
27. J.F. Santaren, M. Rico, J. Guilleme, A. Ribera, Thermal and ^{13}C-NMR study of the dynamic structure of 1-palmitoyl-2-oleoyl-sn-glycero-3-phosphocholine and 1-oleoyl-2-palmitoyl-sn-glycero-3-phosphocholine in aqueous dispersions. Biochim. Biophys. Acta **687**, 231–237 (1982). https://doi.org/10.1016/0005-2736(82)90551-X
28. J. Schaefer, E.O. Stejskal, R. Buchdahl, High-resolution carbon-13 nuclear magnetic resonance study of some solid, glassy polymers. Macromolecules **8**, 291–296 (1975). https://doi.org/10.1021/ma60045a010
29. D.L. VanderHart, W.L. Earl, A.N. Garroway, Resolution in ^{13}C NMR of organic solids using high-power proton decoupling and magic-angle spinning. J. Magn. Reson. **44**, 361–401 (1981). https://doi.org/10.1016/0022-2364(81)90178-5
30. B.V. Cheney, D.M. Grant, Carbon-13 magnetic resonance. VIII. The theory of carbon-13 chemical shifts applied to saturated hydrocarbons. J. Am. Chem. Soc. **89**, 5319–5327 (1967). https://doi.org/10.1021/ja00997a002
31. W.L. Earl, D.L. VanderHart, Observations in solid polyethylenes by carbon-13 magnetic resonance with magic angle sample spinning. Macromolecules **12**, 762–767 (1979). https://doi.org/10.1021/ma60070a045
32. A. Nowacka, S. Douezan, L. Wadsö, D. Topgaard, E. Sparr, Small polar molecules like glycerol and urea can preserve the fluidity of lipid bilayers under dry conditions. Soft Matter **8**, 1482–1491 (2012). https://doi.org/10.1039/C1SM06273E
33. T.M. Ferreira, F. Coreta-Gomes, O.H.S. Ollila, M.J. Moreno, W.L.C. Vaz, D. Topgaard, Cholesterol and POPC segmental order parameters in lipid membranes: solid state ^{1}H–^{13}C NMR and MD simulation studies. Phys. Chem. Chem. Phys. **15**, 1976–1989 (2013). https://doi.org/10.1039/C2CP42738A
34. Q.D. Pham, D. Topgaard, E. Sparr, Cyclic and linear monoterpenes in phospholipid membranes: phase behavior, bilayer structure, and molecular dynamics. Langmuir **31**, 11067–11077 (2015). https://doi.org/10.1021/acs.langmuir.5b00856
35. V. Jagalski, R. Barker, D. Topgaard, T.G. Pomorski, B. Hamberger, M. Cárdenas, Biophysical study of resin acid effects on phospholipid membrane structure and properties. Biochim. Biophys. Acta, Biomembr. **1858**, 2827–2838 (2016). https://doi.org/10.1016/j.bbamem.2016.08.008
36. Q.D. Pham, A. Wolde-Kidan, A. Gupta, A. Schlaich, E. Schneck, R.R. Netz, E. Sparr, Effects of urea and TMAO on lipid self-assembly under osmotic stress conditions. J. Phys. Chem. B **122**, 6471–6482 (2018). https://doi.org/10.1021/acs.jpcb.8b02159
37. J.M. Andersson, Q.D. Pham, H. Mateos, S. Eriksson, P. Harryson, E. Sparr, The plant dehydrin Lti30 stabilizes lipid lamellar structures in varying hydration conditions. J. Lipid Res. **61**, 1014–1024 (2020). https://doi.org/10.1194/jlr.RA120000624
38. S. Fridolf, Q.D. Pham, J. Pallbo, K. Bernfur, S. Linse, D. Topgaard, E. Sparr, Ganglioside GM3 stimulates lipid-protein co-assembly in α-synuclein amyloid formation. Biophys. Chem. (2023). https://doi.org/10.1016/j.bpc.2022.106934
39. D.L. VanderHart, Influence of molecular packing on solid-state ^{13}C chemical shifts: the *n*-alkanes. J. Magn. Reson. **44**, 117–125 (1981). https://doi.org/10.1016/0022-2364(81)90195-5
40. M. Adam-Berret, C. Rondeau-Mouro, A. Riaublanc, F. Mariette, Study of triacylglycerol polymorphs by nuclear magnetic resonance: effects of temperature and chain length on relaxation parameters. Magn. Reson. Chem. **46**, 550–557 (2008). https://doi.org/10.1002/mrc.2213
41. C. Lopez, C. Bourgaux, P. Lesieur, M. Ollivon, Coupling of time-resolved synchrotron X-ray diffraction and DSC to elucidate the crystallisation properties and polymorphism of triglycerides in milk fat globules. Lait **87**, 459–480 (2007). https://doi.org/10.1051/lait:2007018

42. N. Arita-Merino, H. van Valenberg, E.P. Gilbert, E. Scholten, Quantitative phase analysis of complex fats during crystallization. Cryst. Growth Des. **20**, 5193–5202 (2020). https://doi.org/10.1021/acs.cgd.0c00416
43. R.L. Johnson, K. Schmidt-Rohr, Quantitative solid-state ^{13}C NMR with signal enhancement by multiple cross polarization. J. Magn. Reson. **239**, 44–49 (2014). https://doi.org/10.1016/j.jmr.2013.11.009
44. Q.D. Pham, G. Carlström, O. Lafon, E. Sparr, D. Topgaard, Quantification of the amount of mobile components in intact stratum corneum with natural-abundance ^{13}C solid-state NMR. Phys. Chem. Chem. Phys. **22**, 6572–6583 (2020). https://doi.org/10.1039/d0cp00079e